

Article

The Olivine Horizon of the Layered Monchegorsk Pluton (Kola Region, Russia): Additional Magma Injection Based on Integrated Geological and Geochronological Data

Victor Chashchin ^{1,*} and Sergey Sergeev ²¹ Geological Institute of the Kola Science Center, RAS, 14 Fersman St., 184209 Apatity, Russia² Karpinsky Russian Research Geological Institute, 74 Sredny Prospect, 199106 Saint Petersburg, Russia; sergey_sergeev@vsegei.ru

* Correspondence: v.chashchin@ksc.ru

Abstract: The paper presents the first SIMS SHRIMP U-Pb data for zircon from an olivine horizon within the Nyud intrusion of the ore-bearing layered Monchegorsk pluton (Monchepluton) in the Kola Region, Russia. A 100–150 m-thick olivine horizon occurs nearly horizontally between the melanocratic and mesocratic norite of the Nyud intrusion, which disturbs its normal cumulus stratigraphic sequence. In addition, the pyroxene-plagioclase hornfels are present at the upper contact with the olivine horizon. Twenty-three zircon grains were extracted from the large-volume olivine plagioclase-orthopyroxene sample and clustered into two populations. The first population of magmatic zircon (n = 8) has a concordant and weighted average ²⁰⁷Pb/²⁰⁶Pb age of 2484.3 ± 5.6 Ma, which characterizes the formation time of the olivine horizon rocks. This serves as evidence of the olivine horizon that forms as a result of additional magma injection, which does not contradict the geological data. The ²⁰⁷Pb/²⁰⁶Pb age of single-grain zircon is 2414 ± 25 Ma, which indicates the time of postmagmatic transformations. The second population of zircon (n = 16) has a concordant and weighted average U-Pb age of 2700.6 ± 4.6 Ma, which indicates zircon absorption by olivine horizon magma probably from the rocks of the Archean greenstone belt.



Citation: Chashchin, V.; Sergeev, S. The Olivine Horizon of the Layered Monchegorsk Pluton (Kola Region, Russia): Additional Magma Injection Based on Integrated Geological and Geochronological Data. *Geosciences* **2023**, *13*, 344. <https://doi.org/10.3390/geosciences13110344>

Academic Editors: Jesus Martinez-Frias, Feng Guo and Marco Viccaro

Received: 6 September 2023

Revised: 12 October 2023

Accepted: 7 November 2023

Published: 9 November 2023



Copyright: © 2023 by the authors. Licensee MDPI, Basel, Switzerland. This article is an open access article distributed under the terms and conditions of the Creative Commons Attribution (CC BY) license (<https://creativecommons.org/licenses/by/4.0/>).

Keywords: SIMS SHRIMP; U-Pb age; olivine horizon; additional magma injection; plagioclase-pyroxene hornfels; Nyud intrusion; Monchepluton

1. Introduction

The Paleoproterozoic (ca. 2.5 Ga) ore-bearing Monchepluton is located in the southern of the Archean Kola Province (Figure 1), within the northeastern part of Fennoscandian Shield. The Monchepluton is a complex layered mafic–ultramafic intrusion consisting of several blocks divided by tectonic faults. They are traditionally referred to as different intrusions with their own names. Generally, the Monchepluton includes seven independent intrusions, for example, Nittis, Kumuzhya, Travyanaya, Sopcha, Nyud, Poaz, and Vuruchuaivench (Figure 2). Despite its relatively moderate size (approximately 50 km²), the Monchepluton has a considerable ore potential. It combines nearly all types of deposits that are typical of layered intrusions. These are chrome, sulfide platinum-group elements (PGEs)-Cu-Ni, and low-sulfide Pt-Pd ores alongside rich vein Cu-Ni ores that are unusual for such intrusions [1,2]. The Monchepluton sulfide PGEs-Cu-Ni and low-sulfide Pt-Pd deposits are divided into two structural types, i.e., basal ones constrained within lower margin parts of intrusions and reef stratiform ones [3]. Despite long-term research on the Monchepluton, some issues regarding its geological structure need additional research. For example, it has long been believed that the Monchepluton had intruded as a result of a single pulse of mafic–ultramafic magmatism [1,4].

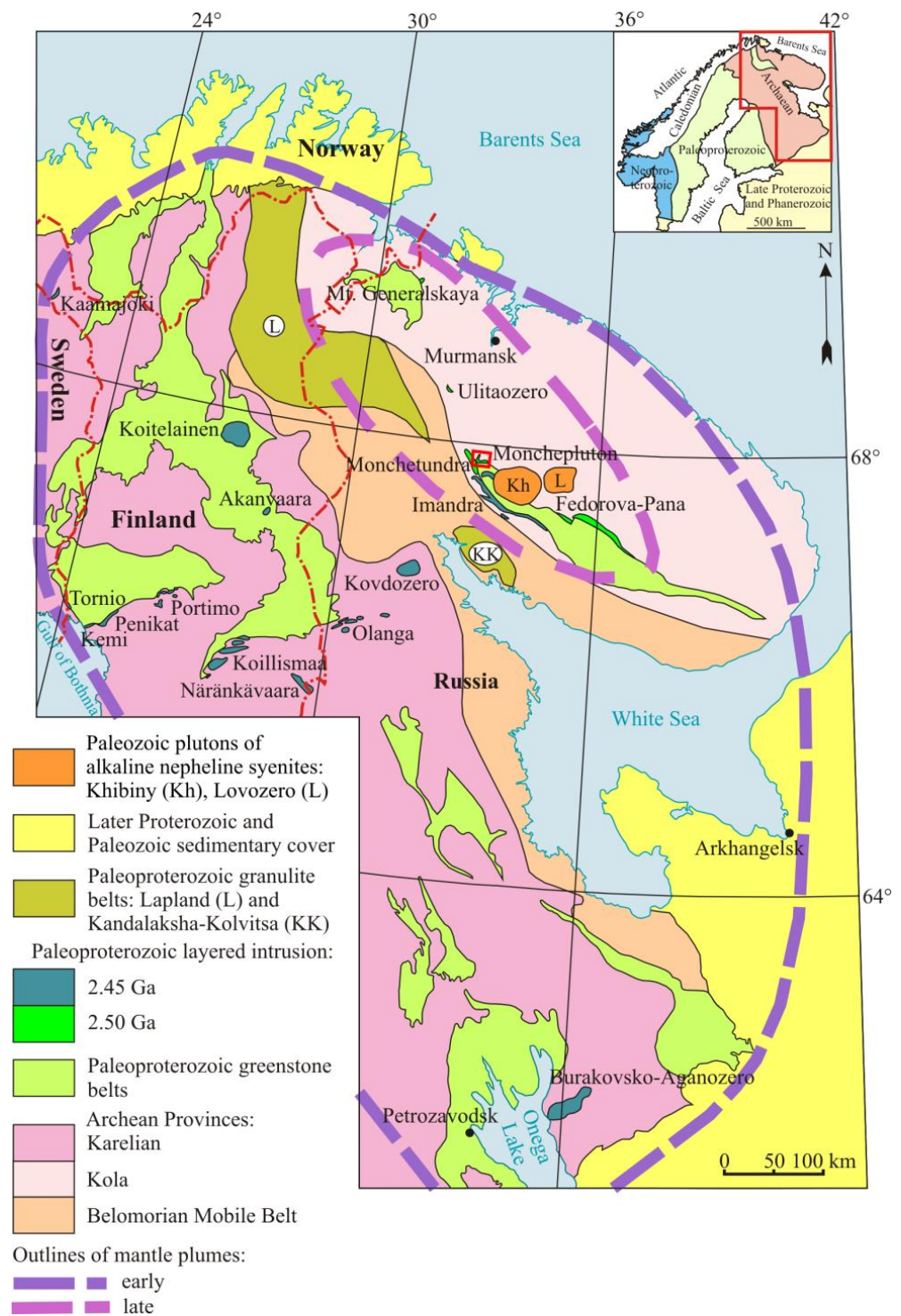


Figure 1. Location scheme of Paleoproterozoic layered intrusion in the northeastern part of the Fennoscandian Shield, modified after [3]. Red square is Figure 2 area. Outlines of mantle plumes after [5].

Later, it was noted [2] that the cumulus stratigraphic sequence of the Monchepluton, which is expressed in a regular change in the composition of rocks from ultramafic to mafic and is characteristic of layered intrusions, is sometimes disrupted. This is particularly evidenced by a presence of thinly layered low-thickness ore horizon named “330 Horizon” among the orthopyroxenite of the upper part of the Sopcha intrusion’s section, and also by a presence of an olivine horizon within the olivine-free norite of the Nyud intrusion (Figure 2). These facts concur with a hypothesis that this horizon may have formed

as a result of additional magma injections occurring later than the Sopcha and Nyud formation time [2].

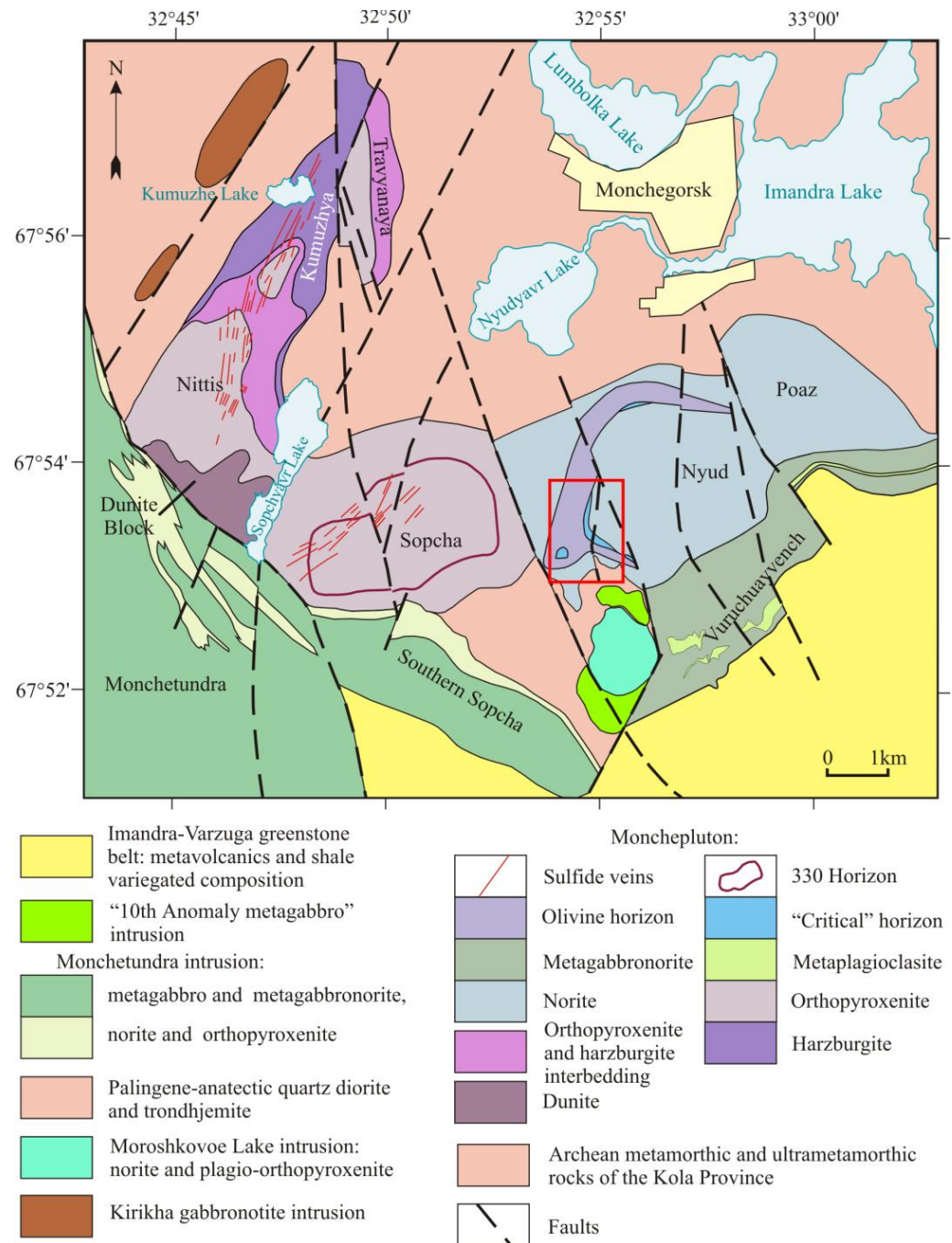


Figure 2. Geological structure of the Monchepluton, modified after [3]. Red square is Figure 3 area.

The formation of PGE reefs including the ore 330 Horizon is a difficult and extensively discussed issue in the scientific community. Of note, petrogenetic models vary from massive magma fractioning to sporadic pressure changes, crustal contamination, and additional magma injection [6–11]. In particular, the additional magma injection model was used to explain the Merensky Reef (Bushveld) genesis [8]. However, this model was not confirmed in the result of a high-precision U-Pb date research [12]. However, this issue needs further study regarding the 330 Horizon.

The presence of an olivine horizon within the olivine-free norite of the Nyud intrusion is another example of the disturbance of the cumulus stratigraphic sequence of the

Monchepluton (Figure 2). This suggests that an additional magma portion was injected during the formation of the Nyud intrusion. Studying the olivine horizon is important because it is associated with the occurrence of PGEs-Cu-Ni ore located in the form of two reef-type ore bodies [3].

The present study aims to examine the geological structure of the olivine horizon with SIMS SHRIMP U-Pb dating of zircon taken from its rocks. The obtained results will significantly improve our understanding of the formation time of the ore-bearing olivine horizon and complement the present data on the geochronology and evolution of the Monchepluton.

2. Regional Geology

The Fennoscandian Shield is the main tectonic structure of Scandinavia and northwestern Russia. Its main volume was developed during the Archean and includes three large tectonic segments, i.e., the Kola and Karelian Provinces, as well as the Belomorian Mobile Belt (Figure 1). The continental crust of the Kola and Karelian Provinces is formed by tonalite-trondhjemite-granodiorite (TTG) granite-gneiss with fragments of metasedimentary and metamagmatic rocks, as well as supracrustal metavolcanic and metasedimentary rocks, which belong to the of Archean greenstone belts.

The Belomorian Mobile Belt lies between the Kola and Karelian Provinces (Figure 1). It comprises the same structural and compositional assemblages as the neighboring provinces, but they experienced significant tectonic transformations in the Neoproterozoic, and Early and Late Paleoproterozoic as a result of the collision of the Kola and Karelian Provinces [13,14]. Within the Belomorian mobile belt, the Lapland and Kandalaksha-Kolvitsa granulite belts are located (Figure 1), which formed as independent tectonic structures in the Late Paleoproterozoic (2.0–1.9 Ga) [15,16].

The Paleoproterozoic magmatism in the Fennoscandian Shield was related to the ascent of an extensive mantle plume that produced numerous layered intrusions, volcanic rift greenstone belt, and mafic dike swarms [5,17–21].

The Fennoscandian layered intrusions are divided into two groups according to their age and correlation with Paleoproterozoic rift volcanic rocks, which reflect the pulsating nature of mantle magmatism. The earlier layered intrusions (ca. 2.50 Ga) are overlain by volcanics and are located only within the Kola region [17,22–24]. This group includes the intrusions of the Mt. Generalskaya and Ulitaozero, Monchegorsk and Fedorova-Pana complexes (Figure 1).

Later layered intrusions (ca. 2.45 Ga) emplaced through the volcanic rocks of greenstone belts are more widespread. They are numerous in Karelian Province (Tornio, Kemi, Penikat, Näränkäväära, Koitelainen, Akanvaara, and Kovdozero intrusions; Portimo, Koilismaa, Olanga, and Burakovsko–Aganozero complexes) [2,25–27] and much less developed in Kola Province (Imandra Complex) [2,24] (Figure 1). There are also numerous massifs of the corona gabbros complex, which formed in the Belomorian Mobile Belt at the same time and are similar in composition and age to the late layered intrusions [28,29]. The layered intrusions of both age groups differ in rock associations, the degree of differentiation, and ore contents. Some of them host Cr, Ni, Cu, PGEs, Ti, and V deposits and manifestations [3,26,27,30–37], parts of which are of commercial importance.

3. Geological Setting

3.1. Geology of the Paleoproterozoic Layered Monchepluton and Intrusions of Its Framing

The Monchepluton represents a typical layered mafic–ultramafic intrusion formed ca. 2.50 Ga ago and contains deposits and manifestations of various sulfide PGE-Cu-Ni (veined, impregnated and injection type), low-sulfide Pt-Pd and Cr ores. It intrudes the Archean granite-gneiss basement and is overlain by the metavolcanics of the Imandra-Varzuga greenstone belt. The Monchepluton is arc-shaped as apparent in the contemporaneous topography at the modern erosion level, having an area of ca. 50 km², and consists of two branches, namely, a northeastern and a nearly east–west one [1,2,38]. The northeastern

branch is about 7 km long and 2 km wide in the middle, comprising the Nittis, Kumuzhya and Travyanaya (NKT) intrusions. The nearly east–west branch is about 11 km long comprising the Sopcha, Nyud, Poaz, and Vuruchuayvench intrusions (Figure 2).

The Monchepluton can be divided into two individual subchambers according to its internal structure. The first subchamber (ultramafic) includes the NKT and Sopcha intrusions, which are up to 1000- and 1200 m-thick, respectively, and have symmetric trough-like shapes with the limbs falling at angles of 20–45° towards the axes. These intrusions consist of ultramafic cumulates of similar internal structure composed of, from bottom to top, lowermost ophitic gabbro-norite (up to 100 m), norite and orthopyroxenite of the marginal zone (10–100 m), harzburgite (100–200 m), interlayering harzburgite and orthopyroxenite (250–400 m), and orthopyroxenite (300–700 m). The 4–6 m-thick thinly (0.4–1.5 m) layered ore horizon 330 occurs in the middle part of the orthopyroxenite sequence in the Sopcha intrusion. The junction zone of the northeastern and nearly east–west branches of the Monchepluton accommodates the 3×1.5 km so-called Dunite Block (Figure 2), which mainly consists of dunite and rare harzburgite on the flanks. Its vertical thickness varies from 100 to 700 m and increases southeastwards. On the upper part of the dunite body, there is a layer-like deposit of chromium ore from the Sopchezero deposit with a length of up to 1200 m and a thickness in the range of 5–35 m [2,30,31]. The ages of dunite and chromium ore of the Dunite Block, determined by the ID-TIMS U-Pb method on single zircon grains, are 2500 ± 10 and 2500 ± 2 Ma, respectively [39].

The second subchamber (mafic) with a complicated shape is formed by the Nyud, Poaz and Vuruchuayvench intrusions with thicknesses of up to 800, 400 and 700 m, respectively. Its structure changes from a trough-like shape in the northern part to a sheet-like shape in the south. The Nyud and Poaz intrusions are characterized by similar cumulus stratigraphic sequences but differ in the thickness of their zones, which are divided into lower and upper ones. Melanonorite and plagiorthopyroxenite make up the lower zones, which are, respectively, 300 m-thick (Nyud) and 70–120 m-thick (Poaz). These rocks are orthocumulates composed of orthopyroxene cumulate and intercumulus plagioclase with rare clinopyroxene poikiloblasts [40]. Leuco-mesocratic norite with gabbro-norite interlayers make up the upper zones, which reach thicknesses of 250 m (Poaz) and 350 m (Nyud), respectively. They are mesocumulates and are composed of cumulus orthopyroxene and plagioclase, locally with a high concentration of clinopyroxene [40]. The Nyud intrusion contains an olivine horizon (Figure 2) that is located between the melanocratic norite of the lower zone and the mesocratic norite of the upper one, which is described in more detail below. The similarity of the cumulus stratigraphic sequences of the Nyud and Poaz intrusions is emphasized by the synchronous ages of the rock formations in their upper zones. Thus, the mesocratic gabbro-norite age of the Nyud intrusion, determined by the ID-TIMS U-Pb method on zircon, is 2493 ± 7 Ma [22], and the gabbro-norite age of the Poaz intrusion, determined by the same method, is 2493 ± 5 Ma [40].

The Vuruchuayvench intrusion is located to the south of the Nyud and Poaz intrusions (Figure 2) and, according to drilling data, completes their magmatic stratigraphy. It is 0.5–2 km wide and extends 6 km northeastwards. In its central part, the intrusion is nearly horizontal; this changes to southeastward dipping at angles of up to 20–30° under the volcanogenic rocks of the Imandra-Varzuga greenstone belt. The Vuruchuayvench intrusion is mainly composed of monotonous mesocratic metagabbro-norite. At its top, it is a 200–400 m-thick banded zone of metagabbro-norite with 5–50 m-thick plagioclase interlayers. The crystallization ages of gabbro-norite and plagioclase obtained by the SIMS SHRIMP U-Pb method on zircon are 2504.2 ± 8.4 and 2507.9 ± 6.6 Ma, respectively [41].

In the southeast, the Monchepluton is in contact with the northwestern end of the Imandra-Varzuga greenstone belt, the total length of which is about 350 km. Here, its stratigraphy consists of three suites (from the bottom up): Kuksha, Seidorechka, and Arvarench suites with thicknesses of up to 400 m, 500 to 2000 m, and ca. 600 m, respectively. Metabasalt of the Kuksha Suite with conglomerates at the bottom overlies the rocks of the Vuruchuayvench intrusion and Archean granitoid basement. The Seidorechka Suite

overlies the Kuksha Suite and is composed of various shales and quartzite at the bottom, as well as mafic and felsic metavolcanites. The Arvarench Suite is located between the Monchetundra and South Sopcha intrusions and is composed of intermediate and felsic metavolcanics. The ID-TIMS U-Pb zircon age of the Seidorechka Suite metarhyodacite is 2448 ± 8 Ma [42], and the Arvarench Suite metadacite age, obtained by SIMS SHRIMP U-Pb zircon dating, is 2430 ± 7 Ma [43].

In the southwest and through the tectonic zone, the Monchepluton is in contact with the Monchetundra intrusion, which has the shape of a strongly elongated oval in plan and is about 30 km long and 2–6 km wide. According to deep structural drilling data, the vertical thickness of its central part is about 2 km, and its upper part and roof are eroded. In the cross-section, the Monchetundra intrusion has a trough shape, with flow textures and primary layering dipping towards its center. Its southeastern branch has its own name, which is the South Sopcha intrusion (Figure 2).

Two zones are distinguished in the internal structure of the Monchetundra intrusion, i.e., a lower norite-orthopyroxenite and an upper leucogabbro-gabbronorite zone [2,44]. The lower zone makes up about 20% of the total volume of the Monchetundra intrusion with a maximum thickness of 450 m. Orthopyroxenite, plagiorthopyroxenite, and mesomelanocratic norite make up the zone. The upper zone of the Monchetundra intrusion accounts for about 80% of its volume with a vertical thickness of 500 to 1400 m. It is composed of mesocratic, medium-grained, less often coarse-grained, intensely amphibolized leucocratic gabbronorite of a massive, flow-textured, and coarse-grained leucogabbro, less often anorthosite, usually occurring in the upper part of the zone.

The ID-TIMS U-Pb zircon ages of orthopyroxenite and norite from the lower zone of the Monchetundra intrusion are 2496.3 ± 2.7 and 2500 ± 2 Ma, respectively [44], and the age of norite from the South Sopcha intrusion is 2504 ± 1 Ma [45]. Within analytical error, these data allow correlation with corresponding rocks of the Monchepluton, which is supported by the similarity of their chemistry of major, trace, and rare earth elements [44].

The metagabbro and gabbronorite ID-TIMS U-Pb ages of the Monchetundra intrusion upper zone vary rather widely from 2505 to 2501 Ma [2], 2476 to 2471 [46,47], and 2456 to 2453 Ma [46–48]. The ID-TIMS U-Pb age of the South Sopcha metagabbro is 2478 ± 20 Ma [45]. Thus, the geological and geochronological data indicate multiphase origins of the Monchetundra and South Sopcha intrusions. The Loypishnyun low-sulfide Pt-Pd deposit is associated with rocks of the lower zone of the Monchetundra intrusion, and the low-sulfide Pt-Pd deposit and the sulfide PGEs-Cu-Ni manifestation are associated with the South Sopcha intrusion [3].

Smaller mafic intrusions are located south of the Nyud intrusion (Moroshkovoe Lake and “10th Anomaly metagabbro”) and northwest of the NKT (Kirikha) (Figure 2). The Moroshkovoe Lake intrusion is round in shape, 1.4×1.1 km in size, and has a vertical thickness varying from 75 m in the north to 350 m in its southern part. It is composed mainly of uralitized norite with interbeds of orthopyroxenite, less frequently of gabbronorite intruded by metagabbro veins. The PGEs-Cu-Ni mineralization was found in the marginal zone of this intrusion [3]. It is assumed that the Moroshkovoe Lake intrusion was previously the southern part of the Nyud intrusion but was separated from it and displaced along faults in a northwestern direction with an offset of about 700 m.

The “10th Anomaly metagabbro” intrusion is located north of the Moroshkovoe Lake intrusion and has an oval shape 1×0.3 km in size (Figure 2). It is mainly composed of medium-grained meso-leucocratic metagabbro with associated titanomagnetite and Pt-Pd mineralization. Similar rocks were discovered in boreholes south of the Moroshkovoe Lake intrusion.

The Kirikha intrusion consists of two bodies. The larger one has a lenticular shape in plan and is elongated in the northeast direction parallel to the NKT intrusion. It is 2.5 km long and 650–700 m wide. The intrusion is mainly composed of mesocratic gabbronorite with olivine-bearing varieties at the bottom and quartz ferro-gabbronorite at the top. The ID-TIMS U-Pb zircon ages of the rocks are 2502 ± 7 Ma for the olivine gabbronorite and

2500 ± 8 Ma for the ferro-gabbronorite [49]. All the intrusions described above, with the exception of the Monchetundra upper zone, belong to the Monchegorsk complex of layered intrusions.

3.2. Olivine Horizon

The sill-like olivine horizon is crescent-shaped in plan and about 5 km long and is present in the western, northern, and southern parts of the Nyud intrusion (Figure 2), between melanocratic and mesocratic norite (Figure 3). Its roof stands out in topographic relief forming distinct exposed terraces in the western (Figure 4a,b) and northern parts of the intrusion. The 100–150-m-thick olivine horizon is almost horizontal. The upper contact of the olivine horizon with the rocks of the “critical” horizon is marked by a thin discontinuous interlayer of pyroxene-plagioclase hornfels (Figure 4c,d). This indicates an intrusive relationship between the rocks of the olivine and “critical” horizons. Its lower contact with the melanocratic norite is usually gradual according to drilling data.

Compositionally, the olivine horizon rocks range from melanocratic norite to orthopyroxenite. The variable contents of cumulus olivine (Fo_{76–84}), varying from rare grains to 30 vol.%, rarely more (Figure 5a–d), represent a distinguishing characteristic of the rocks of the olivine horizon. Often, the highest contents of olivine are noted in the rocks near the roof of the horizon and its bottom. For example, the olivine content traced along the outcrop 425 increases from 10–15 to 25 vol.% (0–3 m) at the beginning and then decreases to 5 vol.% (3–5 m). An inverse distribution is registered in the lower contact zone of the olivine horizon, revealed by borehole BH-23 (location shown in Figure 3). Here, the olivine horizon thickness is 76 m. Within the 0–40 m range, the olivine content gradually decreases from 10 to 2–3 vol.%, then increases up to 30 vol.%. At contact with the hornfels, the plagioclase-orthopyroxenite becomes irregularly grained with a fine-grained groundmass and larger olivine grains (Figure 5b). Cumulus orthopyroxene (En_{74–82}), forming 1–2 mm-sized tabular crystals, is the main rock-forming mineral of the olivine horizon’s rocks (Figure 5a,c). Plagioclase (up to 10 vol.%) is usually found in the intercumulus of cumulus olivine and orthopyroxene and has a variable composition (An_{42–76}) (Figure 5a–d). The presence of large poikiloblastic clinopyroxene (En_{43–48}Fe_{8–13}Wo_{40–48}), ranging from 2 to 5 vol.%, is typical of all the rocks of the olivine horizon (Figure 5d). Locally occurring xenoliths within the olivine horizon (30 m above its bottom) are melanocratic poikilitic norite of the lower zone of the Nyud intrusion.

Located in the roof of the olivine horizon, the up to 60 m-thick and 1.2 km-long “critical” horizon pinches out eastwards after 400 m according to drilling data (Figure 3). The “critical” horizon has a complex internal structure and consists of an irregular alternation of melano- and mesocratic norite, and gabbronorite with interbeds of leucocratic norite and orthopyroxenite. Near the contact with the rocks of the olivine horizon, fine-grained gabbronorite is developed (Figure 5e), and the contact itself is marked by a thin layer of hornfels (Figure 4e,f), which are identical in composition to gabbronorite (Figure 5f). Schliers and veins of pegmatoid gabbronorite developed widely in the rocks of the “critical” horizon. Their ID-TIMS U-Pb zircon age is 2504.4 ± 1.5 Ma [17], and 2500 ± 5 Ma for zircon and baddeleyite [2,23]. The origin of the “critical” horizon remains disputable. One of the existing explanations suggests that it was formed as a result of the injection of additional magma [50]. Another suggestion is that the “critical” horizon is a result of the mixing of ultramafic and mafic melts [2].

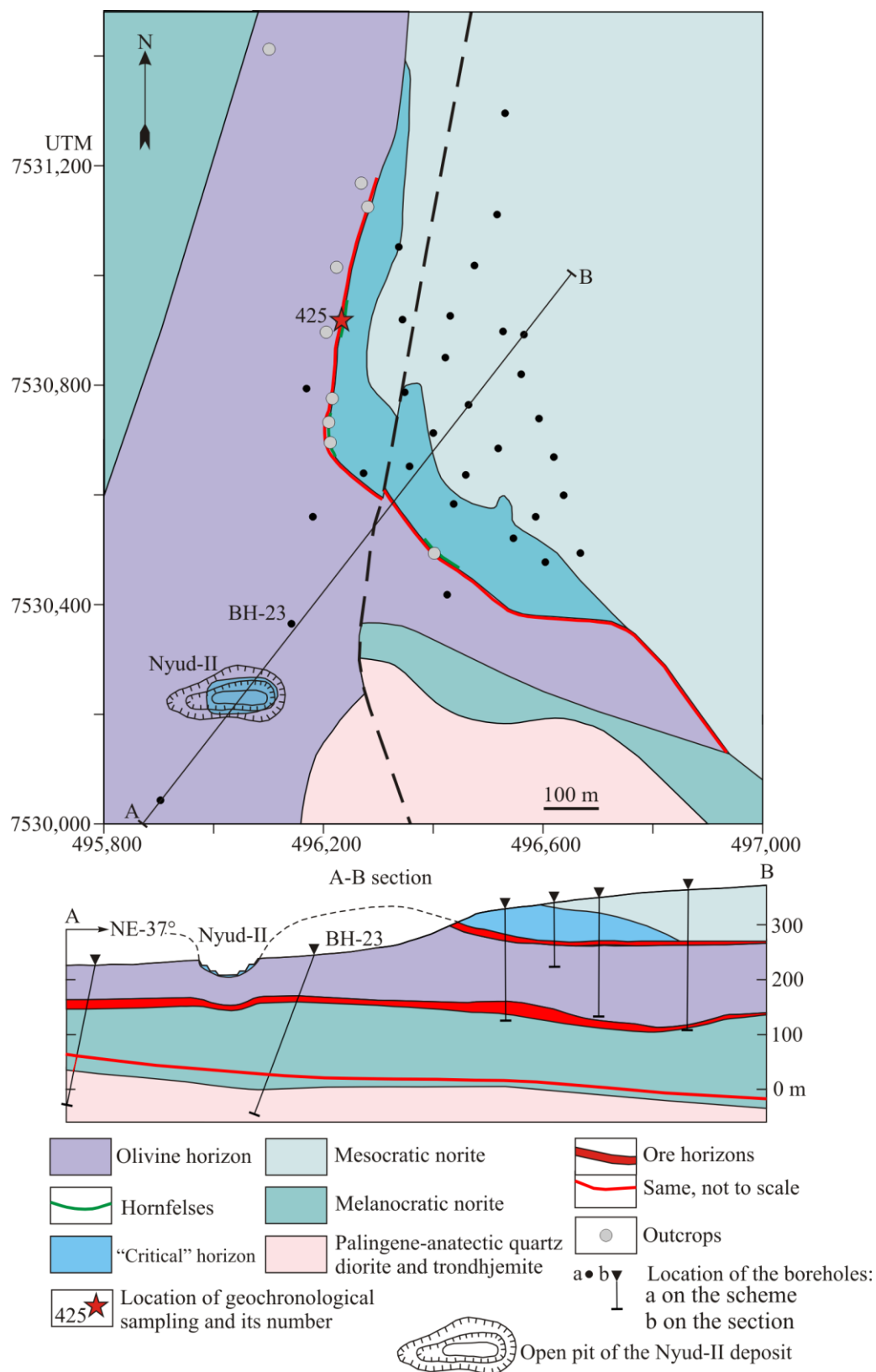


Figure 3. Scheme of the geological structure of the Terrace site of the Nyud intrusion, and section along the A-B line, modified after [51].

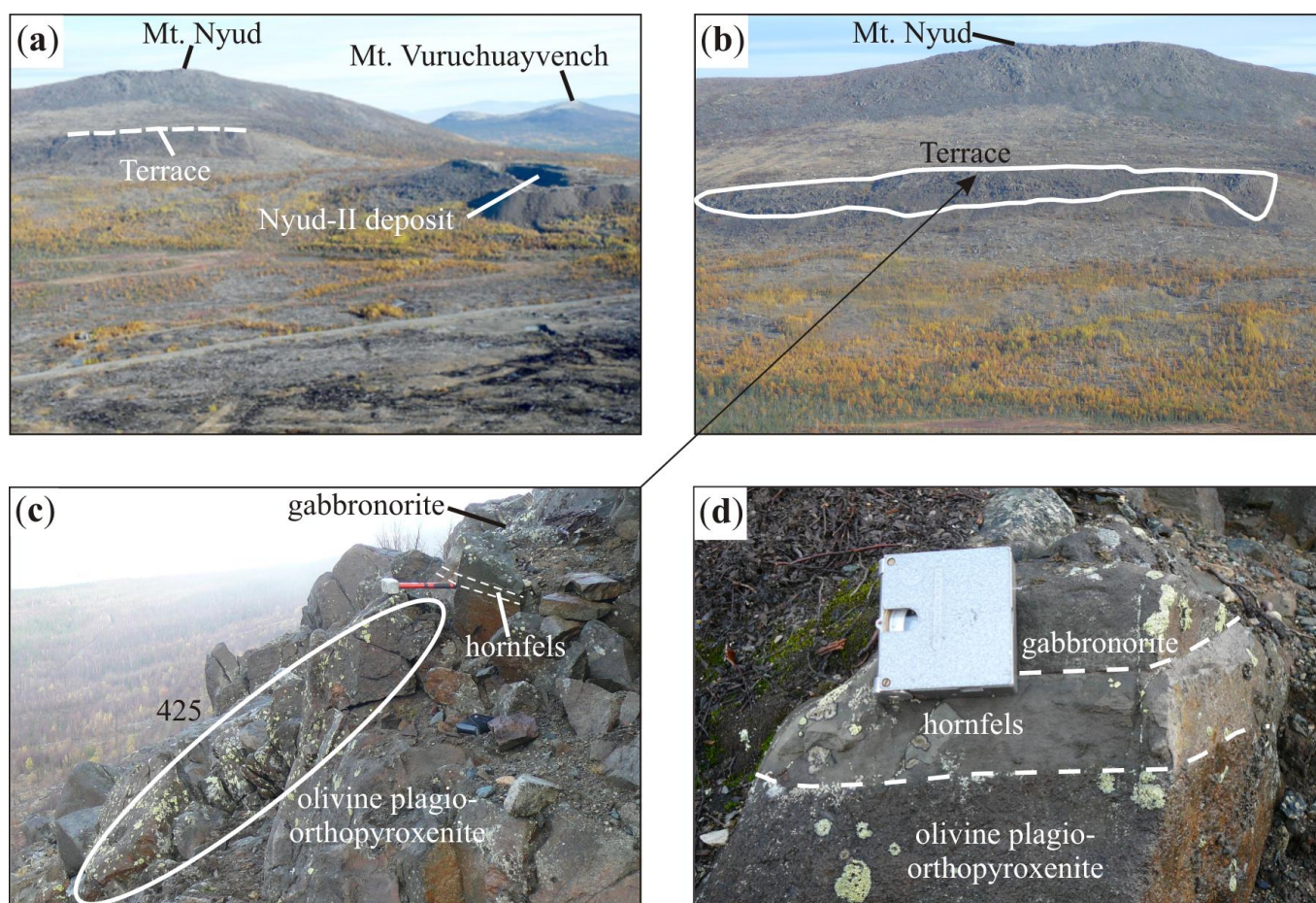


Figure 4. Field photographs: (a) panorama of the terrace site; (b) outcrops of olivine horizon along the slope of the Terrace; (c) outcrop 425 of the olivine horizon at the contact with gabbronorite of the “critical” horizon through a layer of hornfels; (d) hornfel layer at the contact of olivine plagiorthopyroxenite and gabbronorite of the “critical” horizon.

The olivine horizon is associated with PGEs-Cu-Ni ores of the upper and lower reefs of the Terrace manifestation (Figure 3) [3]. The upper reef is confined to the roof of the olivine orthopyroxenite forms by a 1 km-long and 10 m-wide, gently-dipping layer that gradually pinches out eastwards. The lower reef occurs at the exocontact of the olivine horizon among melanocratic poikilitic norite of the lower part of the Nyud intrusion (Figure 3). This reef extends about 1.5 km and has a variable thickness of up to 20 m in the western part of the reef, but smoothly reduces eastwards, averaging approximately 10 m.

Sulfide mineralization in both reefs reaches 1–3 vol.% as fine or medium impregnations and rarely as 1–5 cm-sized nests. The main ore minerals are pyrrhotite, pentlandite and chalcopyrite with subordinate amounts of pyrite, titanomagnetite, ilmenite, and chromite. The platinum-group minerals (PGMs) in both reefs are similar and are Pt and Pd tellurobismuthides [3]. In addition to the reef-type ore in the area, there is the small Nyud-II nested-disseminated sulfide PGEs-Cu-Ni deposit, which occurs in association with leuconorite and gabbronorite of the “critical” horizon; mining was abandoned in the 1970s (Figures 3 and 4) [51].

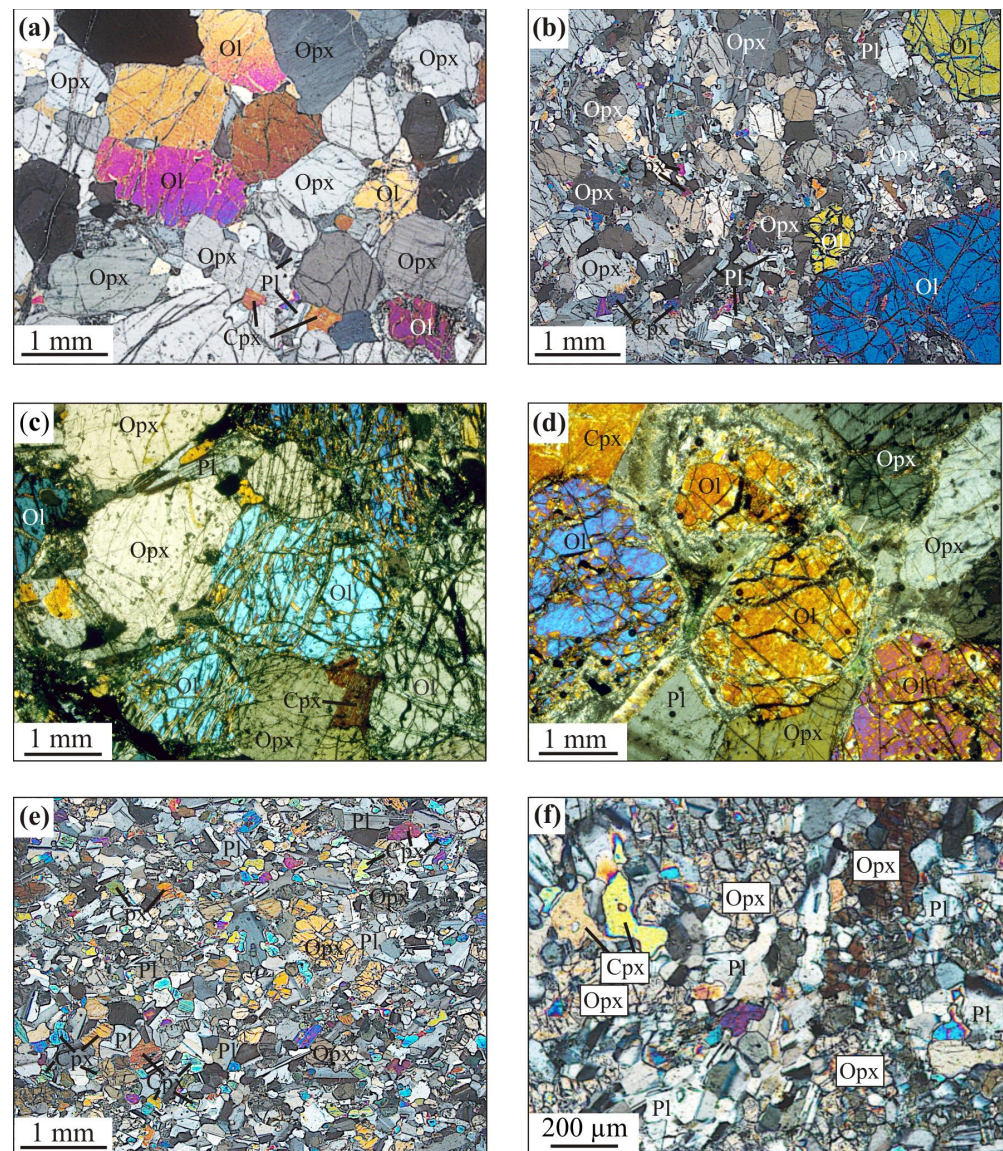


Figure 5. Cross-polarized transmitted-light photomicrographs of thin section: (a) olivine plagiorthopyroxenite 5 m from the upper contact (sample 425); (b) inequigranular plagiorthopyroxenite with olivine 1 m from the upper contact (sample 425/5); (c) olivine orthopyroxenite of the southeastern part of the olivine horizon (sample 428/2); (d) olivine plagiorthopyroxenite 10 m from the lower contact (sample BH-23/67.3); (e) fine-grained “critical horizon” gabbro-norite 1 m from the contact with the olivine horizon (sample 425/8); (f) pyroxene-plagioclase hornfels. Mineral abbreviations after [52]: Ol—olivine, Opx—orthopyroxene, Pl—plagioclase, Cpx—clinopyroxene.

4. Materials and Methods

The object of our study was an outcrop of olivine plagiorthopyroxenite of the olivine horizon, from which a large-volume geochronological sample 425 weighing 21.5 kg was taken. Its location is shown in Figure 3. Twenty-three zircon grains were isolated from it by the standard separation technique using electromagnets of various power and heavy liquids for U-Pb isotope studies. Geochronological studies were performed by way of secondary ion mass spectrometry on a sensitive high-resolution ion micro probe instrument (or SIMS SHRIMP) at the Center for Isotope Research (CRI) of VSEGEI (Saint Petersburg) following the method described in Williams [53] and adapted for CIR [54].

The microscopically hand-picked zircons were mounted in an epoxy disk (as 2.5 cm diameter frame) together with the international zircon standards (TEMORA and 91500),

then polished approximately to half of the grain’s thickness and coated with gold. Further, the zircon grains were documented using a scanning electron microprobe (SEM) (CamScan MX2500 with CLI/QUA2) for cathodoluminescence (CL) and back-scattered electron (BSE) imaging to study the internal zircon structure and to select possible targets. CL and BSE images allowed us to select homogeneous domains for analysis, which were inclusion-free with no secondary modifications and/or mechanical damage. The analysis points (craters) on the dated grains are shown in Figure 6a.

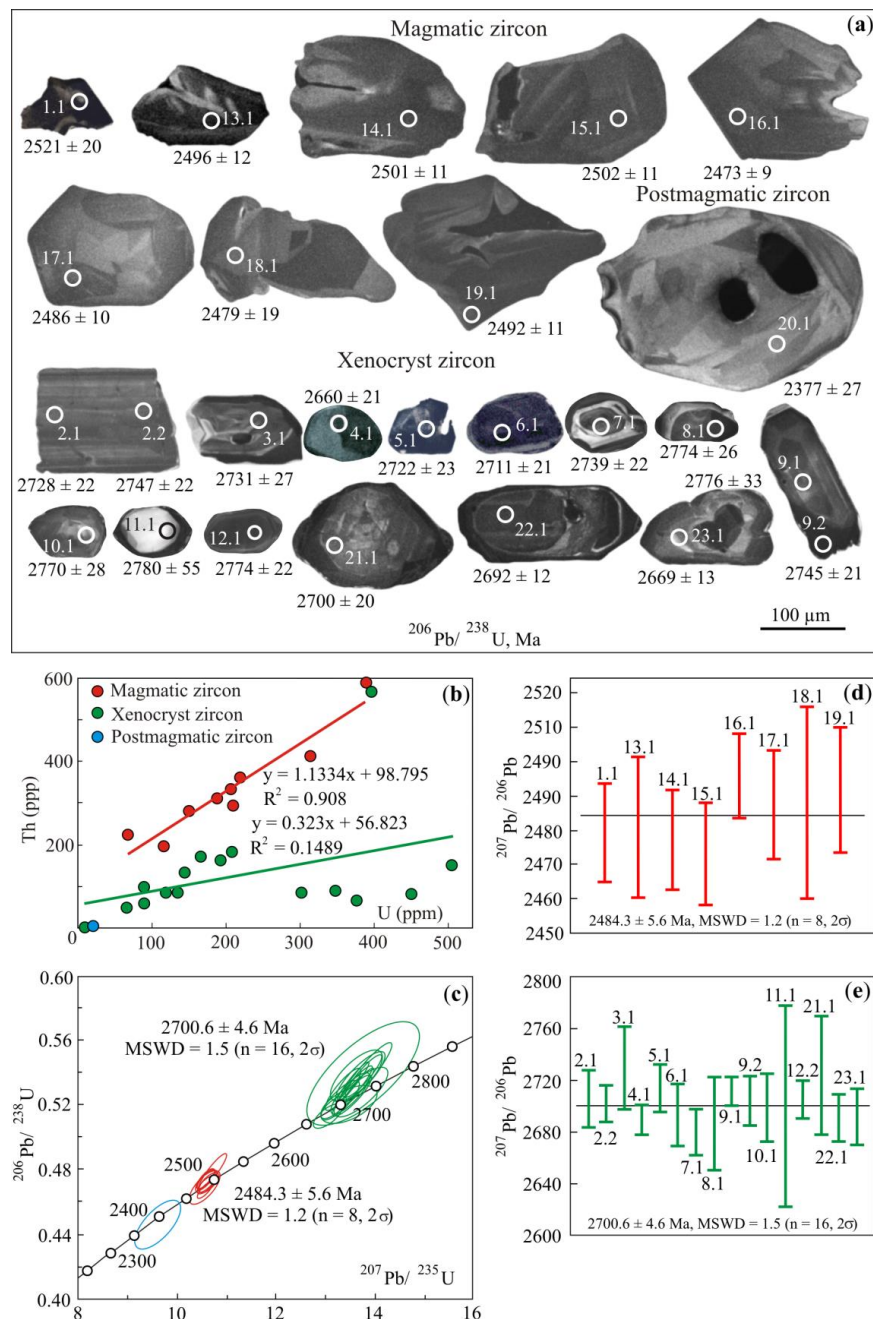


Figure 6. U-Pb dating results for zircon from sample 425 of olivine plagio-orthopyroxenite of the Nyud intrusion: (a) CL images of magmatic, postmagmatic, xenocryst zircon with location and analytical craters (diameter 30 μm), and $^{206}\text{Pb}/^{238}\text{U}$ ages; (b) Th (ppm) versus U (ppm) plot for magmatic and xenocryst zircon; (c) Concordia plot for magmatic, postmagmatic, and xenocryst zircon, $^{207}\text{Pb}/^{206}\text{Pb}$ weighted average ages for (d) magmatic and (e) xenocryst zircon. Colours as for (b).

The intensity of the primary O^{2-} ion beam was ~ 4 nA, and the spot diameter was approximately $30\ \mu\text{m}$ at the $2\ \mu\text{m}$ pit depth. The U/Pb ratios were normalized to that in the Temora standard zircon (0.0668) corresponding to the $^{206}\text{Pb}/^{238}\text{U}$ age of 416.75 ± 0.24 Ma [55]. The 91500 standard zircon with uranium content of 81.2 ppm and a $^{206}\text{Pb}/^{238}\text{U}$ age of 1062 Ma [56] was used as a concentration standard. The raster one-minute cleaning of the rectangular ($50 \times 65\ \mu\text{m}$) mineral area before the dating procedure allowed for minimizing the surface contamination. The obtained data were processed using SQUID software [57].

The errors in single tests (ratios and ages) are given at a 1σ level while the errors of calculated ages, including those that are concordant, are provided at a 2σ level. The Ahrens-Wetherill diagrams with Concordia plots [58] were plotted using the ISOPLOT/EX software [59]. The correction for non-radiogenic Pb was made on the measured ^{204}Pb and modern isotope Pb composition in the Stacey–Kramers model cited in [60].

5. Results

Overall, twenty-five U-Pb isotope analyses were performed on all separated 23 zircon crystals. Table S1 and Figure 6 show these results. All representative zircon grains are homogeneous, characterized by the absence of a significant impact of secondary processes on the U-Pb isotope system. All obtained ages are concordant, since the independent $^{206}\text{Pb}/^{238}\text{U}$ and $^{207}\text{Pb}/^{235}\text{U}$ isotope ages overlap within analytical uncertainties. According to the morphology and isotopic compositions, the studied zircons can be divided into two populations.

The first population of zircon comprises eight short-prismatic zircon grains with a size of 100×65 to $265 \times 165\ \mu\text{m}$ and an elongation coefficient of 1.3 to 2.3 (Figure 6a). They are characterized by rough zoning and the presence of fluid inclusions, without visible cores and shells, sometimes with well-preserved facets.

The second population of zircon is represented by fourteen homogenous zircon grains. They are long- and short-prismatic partially resorbed crystals with preserved crystallographic facets (Figure 6a, grains 9 and 22) with sizes of 75×65 to $215 \times 85\ \mu\text{m}$ and elongation coefficients varying from 1.2 to 2.8 (Figure 6a).

The single zircon grain with the largest size ($300 \times 210\ \mu\text{m}$, elongation coefficient of 1.4) (Figure 6a, grain 20) has partially preserved crystallographic facets and resorption of the grain outer surface containing mineral inclusions.

The zircon in the first population is geochemically homogenous and shows relatively moderate variability of U and Th contents from 68 to 389 ppm U and 196 to 588 ppm Th, respectively, and a high positive correlation coefficient between them (Figure 6b). The average contents are as follows ($n = 8$): U = 207 ppm, Th = 333 ppm, and Th/U = 1.61. A concordant and weighted average $^{207}\text{Pb}/^{206}\text{Pb}$ age of 2484.3 ± 5.6 Ma (MSWD = 1.2, $n = 8$) was obtained for this zircon population (Figure 6c,d). For the concordate, we take such an age when the ellipses of analytical errors intersect the concordia. This is confirmed by the low degree of discordance, varying from -1.7 to 0.9% (Table S1). The obtained age is interpreted as the time of magmatic crystallization of zircon and, accordingly, of the Nyud intrusion olivine horizon.

For the second zircon population, significant variations in U and Th contents are determined in ranges of 10–505 ppm and 1–567 ppm, respectively (Table S1), with no correlation observed between them (Figure 6b). The average contents are as follows ($n = 16$): U = 225 ppm, Th = 130 ppm, and Th/U = 0.58. This zircon population has a concordant and weighted average $^{207}\text{Pb}/^{206}\text{Pb}$ age of 2700.6 ± 4.6 Ma (MSWD = 1.5, $n = 16$) (Figure 6c,e). The concordant age is confirmed by the intersection of the Concordia plots by all ellipses of analytical errors, as well as by the low value of the degree of concordance, varying from -3.1 to 0.9 (Table S1). The obtained results indicate that zircons of the second population are xenocrystic and were probably captured from rocks of the Archean greenstone belt.

The low contents of U = 21 ppm, Th = 6 ppm and Th/U = 0.3 were determined for zircon grain 20 (Table S1). Its $^{207}\text{Pb}/^{206}\text{Pb}$ age is 2414 ± 25 Ma (Table S1). We believe that this age may indicate the time of postmagmatic transformations of the olivine horizon rocks.

6. Discussion

6.1. Geological Features of the Olivine Horizon

The olivine horizon occurs between olivine-free orthocumulates of the lower zone of the Nyud intrusion and mesocumulates of the upper zone, disturbing their regular cumulus stratigraphy sequence. Moreover, a low-power hornfel interlayer is developed at the contact zone of the olivine horizon and the “critical” horizon rocks, having formed as a result of the thermal impact of the olivine horizon magma on host rocks of the “critical” horizon. These facts provide strong evidence in favor of additional later injection of the olivine horizon parental magma into a magmatic chamber of the Nyud intrusion. The internal structure of the olivine horizon is characterized by the absence of layering and by irregular distribution of olivine in the horizon rocks. This may indicate a turbulent (chaotic) character of flow olivine horizon parental magma. Such a kind of flow is usually a feature of low-viscosity magma, which is typical of mafic magma and occurs when the magma flow speed increases in a chamber of proper power [61]. Moreover, the turbulence often occurs with the pressure difference and may be connected to variability in the feeder diameter, for example, when the feeder becomes narrower near the magmatic chamber.

6.2. Zircon Morphology and U, and Th Contents

The morphologies of two studied populations of zircon grains from the olivine horizon are notably different. The magmatic zircon is represented by deformed grains and individual grains with partially preserved facets (Figure 6a). Such forms probably indicate a complicated zircon evolution that happened both in the turbulent magmatic flow and in relatively calm crystallization settings.

The xenocryst zircon is morphologically represented by prismatic bipyramid crystals that sometimes feature a single pyramid and are variously resorbed (Figure 6a). Such variations of zircon shape are common for xenocryst crystals in fluid-rich system settings [62]. Of note, the presence of idiomorphic individual grains is likely to indicate their formation during the amphibolite facies metamorphism, which is inherent in the Archean greenstone belts of the Kola province.

The post-magmatic zircon is of the biggest size and contains irregular domains that may have been developed during the recrystallization; the latter was facilitated by water fluids separated from magma in the deep [62].

The Th and U contents in zircon are a sensitive indicator for a zircon crystallization medium and are more than likely to occur as isomorphic admixtures in the zircon structure [63]. The magmatic zircon is characterized by the U content within the 68–389 ppm range and Th content within the 196–588 ppm range with an average Th/U ratio of 1.61 (Table S1). The range of contents of such incoherent elements as U and Th in the magmatic zircon most likely indicates their variations during the fractioning of parental magma of the olivine horizon.

The xenocryst zircons are characterized by the widest range of U and Th contents (10–505 and 1–567 ppm, respectively, Table S1), and this may be associated with different compositions of rocks (from mafic to asid ones) of the Archean greenstone belt, which it was extracted from.

6.3. Geochronology and Formation Model of the Olivine Horizon

The published geochronological data on the Nyud intrusion rocks fall in the range of 2493–2504 Ma [2,17,22,23]. Of all these ages, only the mesocratic gabbro-norite age of 2493 ± 7 Ma [22] has a direct bearing on the cumulus stratigraphy of the Nyud intrusion, characterizing its upper zone. It can be argued that the upper frontier of the synchronously formed Nyud and Poaz intrusions is 2493 Ma based on the similar age (2493 ± 5 Ma) [40]

of the upper zone gabbro-norite of the Poaz intrusion. At the same time, the ages of 2504.4 ± 1.5 Ma [17] and 2500 ± 5 Ma [2,23] of the vein complex pegmatoid gabbro-norite of the “critical” horizon, which does not belong to the cumulus stratigraphy of the Nyud intrusion, cannot serve as a reliable age benchmark for its formation.

Regarding the age of the bottom part of the Nyud intrusion, the SHRIMP U-Pb dating results for the metadiorite [64] should be examined more thoroughly. These rocks, which we assume to be palingene-anatectic quartz diorite and trondhjemite, occur in the exocontact of the Nyud intrusion. They are exposed in a series of outcrops north of the “10th Anomaly metagabbro” intrusion and have also been discovered in some recent boreholes drilled in the southern part of the Nyud intrusion. The age of this diorite obtained using SIMS SHRIMP U-Pb dating of zircon and baddeleyite is 2498 ± 6 Ma [64] and, according to the authors of this work, they are part of the “10th Anomaly metagabbro” intrusion. However, the results of recent drilling show that these diorites are not always spatially associated with metagabbro but are invariably found in the exocontact of the Nyud intrusion. Moreover, locally, the metagabbro veins traverse the diorite. Taking into account the structural position of the diorites, we believe that they are genetically related to the injection of the Nyud intrusion and were formed as a result of a thermal impact on the underlying host rocks, possibly the Archean greenstone belt. Therefore, the diorite age of 2498 ± 6 Ma indirectly reflects the magmatic event associated with the emplacement of the Nyud intrusion. Therefore, the age of formation of the Nyud intrusion can be limited to the range 2498–2493 Ma or a narrower interval, taking into account the age determination errors.

Consequently, the relevant age of igneous zircons of the first population obtained by us from a sample of the olivine horizon of the Nyud intrusion (2484.3 ± 5.6 Ma) is younger than the rocks of the Nyud intrusion. This result is fully consistent with the geological data on the intrusive relationship of the olivine horizon with the overlying host norite, as evidenced by the presence of hornfels at the top of the olivine horizon. In addition, the cumulus stratigraphic sequence of the Nyud intrusion is disturbed by the presence of the olivine horizon, which lies between the olivine-free melanocratic norite at the bottom and the mesocratic norite at the top. In accordance with the principle of cumulus stratigraphy, this indicates that the formation of the Nyud intrusion was not a single event but rather was accompanied by the injection of a later portion of the olivine horizon parental melt. Therefore, our idea that the olivine horizon was formed as a result of the injection of an additional portion of magma at the stage of magmatic activation following the formation of the largest part of Monchepluton is quite reasonable.

Besides the Monchepluton, the Fedorova Tundra layered intrusion, which is part of the Fedorova-Pana complex (Figure 1), is known to host younger intrusive phases, including ore-bearing gabbro-norite. It occurs in the intrusion’s marginal zone and shows intrusive relationships with rocks of the layered series, whose age was determined by the ID-TIMS U-Pb method on zircon in the range of 2526 ± 8 – 2507 ± 11 Ma [65]. The age of ore-bearing gabbro-norite obtained using the ID-TIMS U-Pb method on zircon is 2485 ± 9 Ma [66] and, within analytical uncertainty, is close to the age of the olivine horizon (this study). Thus, the injection of younger intrusive phases took place between the formation of two age groups of layered intrusions.

The second population of zircons with a U-Pb age of 2700.6 ± 4.6 Ma is clearly xenocrystic and was captured during the injection of olivine horizon magma through the rocks of the Archean Tersko-Allarechka greenstone belt. Located to the south of the Monchepluton, this belt consists of three suites (from the bottom up): the Vochelambina, the Kislaya Guba and the Vite Guba Suites, with thicknesses of 400–650, ca. 3000 and 2000 m, respectively [67]. Of all these suites, only the felsics metavolcanics of the Kislaya Guba Suite yielded a U-Pb zircon age of 2718 ± 10 Ma [67]. Therefore, we assume that the 2718 ± 10 Ma age of the zircon xenocrysts could originate from the rocks of the younger Vite Guba Suite, which constitute the youngest elements of the stratigraphy of the Tersko-Allarechka greenstone belt.

Thus, the results of the study indicate that the sill-like olivine horizon of the Nyud intrusion was formed as a result of the injection of additional portions of magma during ca. 2484 Ma. This magma entered through a narrowing feeder channel, which contributed to a sharp increase in flow speed and led to a turbulent flow of magma.

7. Conclusions

The geological features and age of the olivine horizon from the Nyud intrusion of the Monchepluton were studied. The olivine horizon is a sill-like body with evidence of magmatic relationships with the overlying and underlying rocks. The absence of layering in the olivine horizon and irregular distribution of olivine are caused by the turbulent flow of low-viscosity magma in the magma chamber.

Two zircon populations have been extracted from a large-volume sample. The magmatic zircon is represented by deformed grains and individual grains with partially preserved facets and without zoning. This indicates that they have been formed as a result of both turbulent magmatic flow and relatively calm crystallization settings. The xenocryst zircon shape is characterized by variously resorbed idiomorphic individual grains. This is possible in rocks metamorphosed in amphibolite facies with fluids and does not contradict the possible extraction of the zircon from the Archean greenstone belt rocks. The biggest individual grain of post-magmatic zircon may have been formed as a result of recrystallization of earlier finer grains.

The range of contents U and Th in the magmatic zircon most probably indicates their variations during the fractioning of the olivine horizon parental magma. The xenocryst zircon features wider ranges of U and Th contents, which may be associated with different compositions of rocks (from mafic to felsic ones) of the Archean greenstone belt, from which it was extracted.

The study resulted in a concordant SIMS SHRIMP U-Pb and weighted average $^{207}\text{Pb}/^{206}\text{Pb}$ age of 2484.3 ± 5.6 Ma for magmatic zircon from the olivine horizon of the Nyud intrusion. This age indicates that the horizon formed as a result of an additional magma injection. The injection happened after the formation of the Nyud intrusion into the norite host and agrees with the field observations.

The presence of xenocryst zircon with a concordant SIMS SHRIMP U-Pb and weighted average $^{207}\text{Pb}/^{206}\text{Pb}$ age of 2700.6 ± 4.6 Ma shows that it was captured from the surrounding host rocks of the Archean greenstone belt as a result of their assimilation with the olivine horizon parent magma.

The age frontier of ca. 2480 Ma is of great importance in the geological history of the Kola Province. At that time, additional melts were introduced into the intrusions of the Monchegorsk and Fedorova-Pana layered complexes, and they are genetically related to Pt-Pd ore concentrations.

Supplementary Materials: The following supporting information can be downloaded at: <https://www.mdpi.com/article/10.3390/geosciences13110344/s1>, Table S1: SHRIMP U-Pb isotope analyzes for zircon from the olivine plagioclase-orthopyroxenite (sample 425) of the Nyud intrusion's olivine horizon.

Author Contributions: Conceptualization, V.C.; methodology, V.C. and S.S., software, S.S.; validation, S.S.; formal analysis, V.C. and S.S.; field investigation, V.C.; writing—original draft preparation, V.C.; writing—review and editing, V.C. and S.S.; visualization, V.C. and S.S.; supervision, V.C.; project administration, V.C. and S.S.; funding acquisition, V.C. All authors have read and agreed to the published version of the manuscript.

Funding: This research received no external funding.

Data Availability Statement: Data are contained within the article and Supplementary Materials.

Acknowledgments: The authors thank P. Serov, E. Kunakkuzin, E. Steshenko, and E. Borisenko (GI KSC RAS, Apatity) for their help in the process of field work; L. Koval (GI KSC RAS, Apatity), who crushed the rock and isolated zircons; O. Pridanova (GI KSC RAS, Apatity), who selected the zircon monofractions; and V. Anatsky (GI KSC RAS, Apatity) for translating the manuscript

into English. Three anonymous reviewers and editor Lewis Armstrong are thanked for their very helpful and benevolent comments, which greatly improved the manuscript. The research was carried out within the framework of project 0226–2019–0053 of the Geological Institute of the Kola Science Center, RAS, Apatity (V.C.).

Conflicts of Interest: The authors declare no conflict of interest.

References

1. Kozlov, E.K. *Rocks Natural Series of Nickel-Bearing Intrusions and Their Metallogeny*; Nauka: Leningrad, Russia, 1973. (In Russian)
2. Smolkin, V.F.; Fedotov, Z.A.; Orsoev, D.A.; Ohnenstetter, D. Ore-bearing layered Monchepluton. In *Layered Intrusion of the Monchegorsk Ore Region: Petrology, Mineralization, Isotopy, Deep Structure. Part 1*; Part 1, Mitrofanov, F.P., Smolkin, V.F., Eds.; Kola Science Center Russian Academy of Sciences: Apatity, Russia, 2004; pp. 36–74. (In Russian with English Abstract).
3. Chashchin, V.V.; Ivanchenko, V.N. Sulfide PGE-Cu-Ni and low-sulfide Pt-Pd ores of the Monchegorsk ore district (Arctic Western Sector): Geology, mineralogy, geochemistry, and genesis. *Russ. Geol. Geophys.* **2022**, *63*, 519–542. [[CrossRef](#)]
4. Eliseev, E.N. Disseminated sulfide mineralization of the Sopcha ore layer. In *Ultrabasic and Basic Intrusions and sulfide Copper-Nickel Deposits of the Moncha*; Eliseev, N.A., Ed.; USSR Academy of Sciences: Leningrad, Russia, 1953; pp. 112–143. (In Russian)
5. Smolkin, V.F.; Kremenetsky, A.A.; Vetrin, V.R. Geological and genetic model of the formation of Paleoproterozoic ore-magmatic systems of the Baltic Shield. *Otechestv. Geol.* **2009**, 54–62. (In Russian)
6. Haughton, D.R.; Roeder, P.L.; Skinner, B.J. Solubility of sulfur in mafic magmas. *Econ. Geol.* **1974**, *69*, 451–467. [[CrossRef](#)]
7. Cameron, E.N. Evolution of the Lower Critical zone, central sector, eastern Bushveld Complex, and its chromite deposits. *Econ. Geol.* **1980**, *75*, 845–871. [[CrossRef](#)]
8. Campbell, I.H.; Naldrett, A.J.; Barnes, S.J. A model for the origin of the platinum-rich sulfide horizons in the Bushveld and Stillwater Complexes. *J. Petrol.* **1983**, *24*, 133–165. [[CrossRef](#)]
9. Lee, C.A.; Butcher, A.R. Cyclicity in the Sr isotope stratigraphy through the Merensky and Bastard Reef units, Atok section, eastern Bushveld Complex. *Econ. Geol.* **1990**, *85*, 877–883. [[CrossRef](#)]
10. Cawthorn, R.G. Pressure fluctuations and the formation of the PGE-rich Merensky and chromitite reefs, Bushveld Complex. *Miner. Depos.* **2005**, *40*, 231–235. [[CrossRef](#)]
11. Maier, W.D.; Barnes, S.-J.; Groves, D.I. The Bushveld Complex, South Africa: Formation of platinum-palladium, chrome- and vanadium-rich layers via hydrodynamic sorting of a mobilized cumulate slurry in a large, relatively slowly cooling, subsiding magma chamber. *Miner. Depos.* **2013**, *48*, 1–56. [[CrossRef](#)]
12. Scoates, J.S.; Wall, C.J.; Friedman, R.M.; Weis, D.; Mathez, E.A.; VanTongeren, J.A. Dating the Bushveld Complex: Timing of crystallization, duration of magmatism, and cooling of the world's largest layered intrusion and related rocks. *J. Petrol.* **2021**, *62*, ega107. [[CrossRef](#)]
13. Kozlov, N.E.; Sorokhtin, N.O.; Glaznev, V.N.; Kozlova, N.E.; Ivanov, A.A.; Kudryashov, N.M.; Martynov, E.V.; Tyuremnov, V.V.; Matyushkin, A.V.; Osipenko, L.G. *Geology of the Archean Baltic Shield*; Nauka: Saint Petersburg, Russia, 2006. (In Russian)
14. Slabunov, A.I.; Balagansky, V.V.; Shchipansky, A.A. Mesoarchean to Paleoproterozoic crustal evolution of the Belomorian province, Fennoscandian Shield, and the tectonic setting of eclogites. *Russ. Geol. Geophys.* **2021**, *62*, 525–546. [[CrossRef](#)]
15. Gaál, G.; Gorbatshev, R. An outline of the Precambrian evolution of the Baltic shield. *Precambrian Res.* **1987**, *35*, 15–52. [[CrossRef](#)]
16. Balagansky, V.V.; Gorbunov, I.A.; Mudruk, S.V. Paleoproterozoic Lapland–Kola and Svecofennian orogens (Baltic Shield). *Vestn. KNTs RAN* **2016**, *3*, 5–11. (In Russian with English Abstract).
17. Amelin, Y.V.; Heaman, L.M.; Semenov, V.S. U–Pb geochronology of layered mafic intrusions in the eastern Baltic Shield: Implication for the timing and duration of Paleoproterozoic continental rifting. *Precambrian Res.* **1995**, *75*, 31–46. [[CrossRef](#)]
18. Lahtinen, R.; Garde, A.A.; Melezhik, V.A. Paleoproterozoic evolution of Fennoscandia and Greenland. *Episodes* **2008**, *31*, 20–28. [[CrossRef](#)] [[PubMed](#)]
19. Puchtel, I.S.; Haase, K.M.; Hofmann, A.W.; Chauvel, C.; Kulikov, V.S.; Garbe-Schönberg, C.-D.; Nemchin, A.A. Petrology and geochemistry of crustally contaminated komatiitic basalts from the Vetreny belt, southeastern Baltic Shield: Evidence for an early Proterozoic mantle plume beneath rifted Archean continental lithosphere. *Geochim. Cosmochim. Acta* **1997**, *61*, 1205–1222. [[CrossRef](#)]
20. Sharkov, E.V.; Bogatkov, O.A.; Krasivskaya, I.S. The role of mantle plumes in the early Precambrian tectonics of the eastern Baltic Shield. *Geotectonics* **2000**, *34*, 85–105.
21. Yang, S.-H.; Hanski, E.; Li, C.; Maier, W.D.; Huhma, H.; Mokrushin, A.V.; Latypov, R.; Lahaye, Y.; O'Brien, H.; Qu, W.-J. Mantle source of the 2.44–2.50-Ga mantle plume-related magmatism in the Fennoscandian Shield: Evidence from Os, Nd, and Sr isotope compositions of the Monchepluton and Kemi intrusions. *Miner. Depos.* **2016**, *51*, 1055–1073. [[CrossRef](#)]
22. Balashov, Y.A.; Bayanova, T.B.; Mitrofanov, F.P. Isotope data on the age and genesis of layered basic-ultrabasic intrusions in the Kola Peninsula and northern Karelia, northeastern Baltic Shield. *Precambrian Res.* **1993**, *64*, 197–205. [[CrossRef](#)]
23. Bayanova, T.B. *Age of the Reverence Geological Complexes of the Kola Region and Duration of Magmatic Processes*; Nauka: Saint Petersburg, Russia, 2004. (In Russian)
24. Chashchin, V.V. Paleoproterozoic complex of layered intrusions of the Kola Peninsula and its metallogeny (Russia). *Geol. Ore Depos.* **1999**, *41*, 114–125.

25. Alapieti, T.T.; Filen, B.A.; Lahtinen, J.J.; Lavrov, V.V.; Smolkin, V.F.; Voitsekhovskiy, S.N. Early Proterozoic layered intrusions in the northeastern part of the Fennoscandian Shield. *Mineral. Petrol.* **1990**, *42*, 1–22. [[CrossRef](#)]
26. Alapieti, T.T.; Lahtinen, J.J. Platinum-group element mineralization in layered intrusions of northern Finland and the Kola Peninsula, Russia. In *The Geology, Geochemistry, Mineralogy and Mineral Beneficiation of Platinum-Group Elements*; Cabri, L.J., Ed.; Canadian Institute of Mining, Metallurgy and Petroleum: Ottawa, ON, Canada, 2002; Volume 54, pp. 507–546. [[CrossRef](#)]
27. Maier, W.D. Geology and petrogenesis of magmatic Ni-Cu-PGE-Cr-V deposits: An introduction and overview. In *Mineral Deposits of Finland*; Maier, W.D., Lahtinen, R., O'Brien, H., Eds.; Elsevier: Amsterdam, The Netherlands; Oxford, UK; Waltham, MA, USA, 2015; pp. 73–92. [[CrossRef](#)]
28. Sharkov, E.V.; Krasivskaya, I.S.; Chistyakov, A.V. Dispersed mafic-ultramafic intrusive magmatism in Early Paleoproterozoic mobile zones of the Baltic Shield: An example of the Belomorian drusite (coronite) complex. *Petrology* **2004**, *12*, 561–582.
29. Krivolutskaya, N.A.; Svirskaya, N.M.; Roshchina, I.A.; Smolkin, V.F.; Mamontov, V.P.; Fanygin, A.S.; Belyatskii, B.V. Geochemical features of the drusite massifs, the central part of the Belomorian mobile belt: I. *Distribution of major and trace elements in the rocks. Geochem. Int.* **2010**, *48*, 465–491. [[CrossRef](#)]
30. Chashchin, V.V.; Galkin, A.S.; Ozeryanskii, V.V.; Dedyukhin, A.N. Sopcha Lake chromite deposit and its platinum potential, Monchegorsk Pluton, Kola Peninsula (Russia). *Geol. Ore Depos.* **1999**, *41*, 460–468.
31. Mokrushin, A.V.; Smolkin, V.F. Chromite mineralization in the Sopchezero deposit (Monchegorsk layered intrusion, Fennoscandian Shield). *Minerals* **2021**, *11*, 772. [[CrossRef](#)]
32. Alapieti, T.T.; Kujanpää, J.; Lahtinen, J.J.; Papunen, H. The Kemi stratiform chromitite deposit, northern Finland. *Econ. Geol.* **1989**, *84*, 1057–1077. [[CrossRef](#)]
33. Fedotov, Z.A.; Smolkin, V.F.; Mokrushin, A.V. The Umbarechka-Umba chromite-bearing norite-gabbro-norite complex. In *Layered Intrusion of the Monchegorsk Ore Region: Petrology, Mineralization, Isotopy, Deep Structure. Part 1*; Mitrofanov, F.P., Smolkin, V.F., Eds.; Kola Science Center Russian Academy of Sciences: Apatity, Russia, 2004; pp. 98–116, (In Russian with English Abstract).
34. Groshev, N.Y.; Rundkvist, T.V.; Karykowski, B.T.; Maier, W.D.; Korzhagin, A.U.; Ivanov, A.N.; Junge, M. Low-sulfide platinum-palladium deposits of the Paleoproterozoic Fedorova-Pana layered complex, Kola Region, Russia. *Minerals* **2019**, *9*, 764. [[CrossRef](#)]
35. Iljina, M.; Maier, W.D.; Karinen, T. PGE-(Cu-Ni) deposits of the Tornio-Näränkävää belt of intrusions (Portimo, Penikat, and Koillismaa). In *Mineral Deposits of Finland*; Maier, W.D., Lahtinen, R., O'Brien, H., Eds.; Elsevier: Amsterdam, The Netherlands; Oxford, UK; Waltham, MA, USA, 2015; pp. 133–164. [[CrossRef](#)]
36. Huhtelen, T. The Kemi chromite deposit. In *Mineral Deposits of Finland*; Maier, W.D., Lahtinen, R., O'Brien, H., Eds.; Elsevier: Amsterdam, The Netherlands; Oxford, UK; Waltham, MA, USA, 2015; pp. 165–178. [[CrossRef](#)]
37. Karinen, T.; Hanski, E.; Taipale, A. Mustavaara V-Fe-Ti oxide deposit. In *Mineral Deposits of Finland*; Maier, W.D., Lahtinen, R., O'Brien, H., Eds.; Elsevier: Amsterdam, The Netherlands; Oxford, UK; Waltham, MA, USA, 2015; pp. 179–195. [[CrossRef](#)]
38. Gorbunov, G.I.; Yakovlev, Y.N.; Goncharov, Y.V.; Gorelov, V.A.; Telnov, V.A. Kola Peninsula nickel-bearing regions. In *Baltic Shield Copper-Nickel Deposits*; Gorbunov, G.I., Papunen, H., Eds.; Nauka: Leningrad, Russia, 1985; pp. 27–93. (In Russian)
39. Chashchin, V.V.; Bayanova, T.B. Sopchezero chromite deposit: Geochemistry and U-Pb age. *Proc. Fersman Sci. Sess. Geol. Inst. KSC RAS* **2021**, *18*, 403–408. [[CrossRef](#)]
40. Chashchin, V.V.; Bayanova, T.B. Cumulus stratigraphy, petrochemistry, and U-Pb age of the layered Poaz intrusion of Monchegorsk pluton, Kola Peninsula. In *Proceedings of the Fersman Scientific Session of the Geological Institute of the Kola Science of the Russian Academy of Sciences, Apatity, Russia, 5–6 April 2023*; pp. 229–235, (In Russian with English Abstract).
41. Rundkvist, T.V.; Bayanova, T.B.; Sergeev, S.A.; Pripachkin, P.V.; Grebnev, R.A. The Paleoproterozoic Vurechuaivench layered Pt-bearing pluton, Kola Peninsula: New results of the U-Pb (ID TIMS, SHRIMP) dating of baddeleyite and zircon. *Dokl. Earth Sci.* **2014**, *454*, 1–6. [[CrossRef](#)]
42. Chashchin, V.V.; Bayanova, T.B.; Levkovich, N.V. Volcanoplutonic association of the early-stage evolution of the Imandra-Varzuga rift zone, Kola Peninsula, Russia: Geological, petrogeochemical, and isotope-geochronological data. *Petrology* **2008**, *16*, 279–298. [[CrossRef](#)]
43. Vrevsky, A.B. Petrology, age, and polychromous sources of the initial magmatism of the Imandra-Varzuga paleorift, Fennoscandian shield. *Petrology* **2011**, *19*, 521–547. [[CrossRef](#)]
44. Chashchin, V.V.; Bayanova, T.B.; Savchenko, Y.E.; Kiseleva, D.V.; Serov, P.A. Petrogenesis and age of rocks from the lower zone of the Monchetundra mafic platinum-bearing massif, Kola Peninsula. *Petrology* **2020**, *28*, 151–182. [[CrossRef](#)]
45. Chashchin, V.V.; Bayanova, T.B.; Mitrofanov, F.P.; Serov, P.A. Low-sulfide PGE ores in Paleoproterozoic Monchegorsk pluton and massifs of its southern framing, Kola Peninsula, Russia: Geological characteristic and isotopic geochronological evidence of polychromous ore-magmatic systems. *Geol. Ore Depos.* **2016**, *58*, 37–57. [[CrossRef](#)]
46. Nerovich, L.I.; Bayanova, T.B.; Savchenko, Y.E.; Serov, P.A.; Ekimova, N.A. New data on geology, petrography, isotopic geochemistry, and PGE mineralization of the Monchetundra massif. *Proc. Murm. State Tech. Univ.* **2009**, *12*, 461–477, (In Russian with English Abstract).
47. Bayanova, T.B.; Nerovich, L.I.; Mitrofanov, F.P.; Zhavkov, V.A.; Serov, P.A. The Monchetundra basic massif of the Kola Region: New geological and isotope geochronological data. *Dokl. Earth Sci.* **2010**, *431*, 288–293. [[CrossRef](#)]
48. Mitrofanov, F.P.; Balagansky, V.V.; Balashov, Y.A.; Gannibal, L.F.; Dokuchaeva, V.S.; Nerovich, L.I.; Radchenko, M.K.; Ryungenen, G.I. U-Pb age of gabbro-anorthosites of the Kola Peninsula. *Dokl. Earth Sci.* **1993**, *331*, 95–98. (In Russian)

49. Chashchin, V.V.; Bayanova, T.B.; Lyulko, M.S. Geologic composition and U–Pb age of the Kirikha gabbro-norite massif—Kola Peninsula, Russia. In Proceedings of the Geology and Geochronology of Rock-Forming and Ore Processes in Crystalline Shields. Proceedings of the All-Russian Conference, Apatity, Russia, 8–12 July 2013; pp. 179–181. (In Russian).
50. Sharkov, E.V. “Critical horizon” of the Monchegorsk pluton—An additional intrusive phase. *Proc. All-Union Mineral. Soc.* **1982**, *111*, 656–664. (In Russian)
51. Chashchin, V.V.; Petrov, S.V.; Kiseleva, D.S.; Savchenko, Y.E. Platinum content and formation conditions of the sulfide PGE-Cu-Ni Nyud-II deposit of the Monchegorsk pluton, Kola Peninsula, Russia. *Geol. Ore Depos.* **2021**, *63*, 87–117. [[CrossRef](#)]
52. Warr, L.N. IMA-CNMNC approved mineral symbols. *Mineral. Mag.* **2021**, *85*, 291–320. [[CrossRef](#)]
53. Williams, I.S. U–Th–Pb geochronology by ion microprobe. In *Applications of Microanalytical Techniques to Understanding Mineralizing Processes*; McKibben, M.A., Shanks, W.C., Ridley, W.I., Eds.; Reviews in Economic Geology; Economic Geology Pub Co.: Socorro, NM, USA; Toronto, ON, Canada, 1998; pp. 1–35.
54. Schuth, S.; Gornyy, V.I.; Berndt, J.; Shevchenko, S.S.; Sergeev, S.A.; Karpuzov, A.F.; Mansfeldt, T. Early Proterozoic U–Pb Zircon Ages from Basement Gneiss at the Solovetsky Archipelago, White Sea, Russia. *Int. J. Geosci.* **2012**, *3*, 289–296. [[CrossRef](#)]
55. Black, L.P.; Kamo, S.L.; Allen, C.M.; Aleinikoff, J.N.; Davis, D.W.; Korsch, R.J.; Foudoulis, C. TEMORA 1: A new zircon standard for U–Pb geochronology. *Chem. Geol.* **2003**, *200*, 155–170. [[CrossRef](#)]
56. Wiedenbeck, M.; Alle, P.; Corfu, F.; Griffin, W.L.; Meier, M.; Oberli, F.; Von Quadt, A.; Roddick, J.C.; Spiegel, W. Three natural zircon standards for U–Th–Pb, Lu–Hf trace element and REE analyses. *Geostand. Geoanalyt. Res.* **1995**, *19*, 1–23. [[CrossRef](#)]
57. Ludwig, K.R. *SQUID 1.02, a User Manual, a Geochronological Toolkit for Microsoft Excel*; Berkeley Geochronology Center Special Publication: Berkeley, CA, USA, 2001.
58. Wetherill, G.W. Discordant uranium-lead ages. *Trans. Am. Geophys. Union* **1956**, *37*, 320–326.
59. Ludwig, K.R. *User’s Manual for Isoplot 3.00, a Geochronological Toolkit for Microsoft Excel*; Berkeley Geochronology Centre Special Publication: Berkeley, CA, USA, 2003.
60. Stacey, J.S.; Kramers, J.D. Approximation of terrestrial lead isotope evolution by a two-stage model. *Earth Planet. Sci. Lett.* **1975**, *26*, 207–221. [[CrossRef](#)]
61. Nair, V.C.A. The instability of convection of magma in the chamber, triggering eruption in volcanoes. *Int. Adv. Res. J. Sci. Engin. Technol.* **2019**, *6*, 1–15. [[CrossRef](#)]
62. Corfu, F.; Hanchar, J.M.; Hoskin, P.W.O.; Kinny, P. Atlas of zircon textures. *Rev. Mineral. Geochem.* **2003**, *53*, 468–500. [[CrossRef](#)]
63. Hoskin, P.W.O.; Schaltegger, U. The composition of zircon and metamorphic petrogenesis. *Rev. Mineral. Geochem.* **2003**, *53*, 27–62. [[CrossRef](#)]
64. Groshev, N.Y.; Pripachkin, P.V.; Malygina, A.V.; Karykowski, B.T.; Rodionov, N.V.; Belyatsky, B.V. Genesis of a magnetite layer in the Gabbro-10 intrusion, Monchegorsk Complex, Kola Region: U–Pb SHRIMP-II dating of metadiorites. *Geol. Ore Depos.* **2018**, *60*, 486–496. [[CrossRef](#)]
65. Groshev, N.Y.; Nitkina, E.A.; Mitrofanov, F.P. Two-phase mechanism of the formation of platinum-metal basites of the Fedorova Tundra intrusion of the Kola Peninsula: New data on geology and isotope geochronology. *Dokl. Earth Sci.* **2009**, *427*, 1012–1016. [[CrossRef](#)]
66. Nitkina, E.A. U–Pb zircon dating of rocks of the platiniferous Fedorova-Pana layered massif, Kola Peninsula. *Dokl. Earth Sci.* **2006**, *408*, 551–554. [[CrossRef](#)]
67. Chashchin, V.V.; Bayanova, T.B.; Levkovich, N.V. The Kislaya Guba formation of the Late Archean Terskii-Allarechensk greenstone belt (Kola Peninsula, Russia): Stratotype and U–Pb age. *Stratigr. Geol. Correl.* **2004**, *12*, 541–552.

Disclaimer/Publisher’s Note: The statements, opinions and data contained in all publications are solely those of the individual author(s) and contributor(s) and not of MDPI and/or the editor(s). MDPI and/or the editor(s) disclaim responsibility for any injury to people or property resulting from any ideas, methods, instructions or products referred to in the content.